Physical Chemistry Chemical Physics c1cp22619c

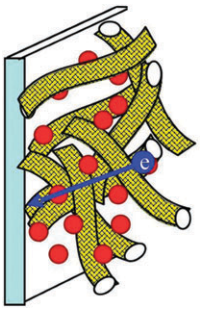

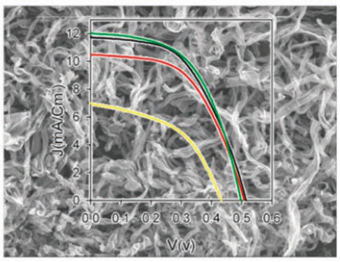

Q1 **Easily manufactured TiO_2 hollow fibers for quantum dot sensitized solar cells**

Mahmoud Samadpour, Sixto Giménez, Azam Iraji Zad,* Nima Taghavinia and Iván Mora-Seró*

We show here that TiO_2 hollow fibers can be introduced as a promising nanostructure to make highly efficient quantum dot sensitized solar cells.

Please check this proof carefully. **Our staff will not read it in detail after you have returned it.** Translation errors between word-processor files and typesetting systems can occur so the whole proof needs to be read. Please pay particular attention to: tabulated material; equations; numerical data; figures and graphics; and references. If you have not already indicated the corresponding author(s) please mark their name(s) with an asterisk. Please e-mail a list of corrections or the PDF with electronic notes attached – do not change the text within the PDF file or send a revised manuscript.

Please bear in mind that minor layout improvements, e.g. in line breaking, table widths and graphic placement, are routinely applied to the final version.

Please note that, in the typefaces we use, an italic vee looks like this: ν, and a Greek nu looks like this: ν.

We will publish articles on the web as soon as possible after receiving your corrections; **no late corrections will be made.**

Please return your **final** corrections, where possible within **48 hours** of receipt, by e-mail to: pccp@rsc.org.

Reprints—Electronic (PDF) reprints will be provided free of charge to the corresponding author. Enquiries about purchasing paper reprints should be addressed via: http://www.rsc.org/publishing/journals/guidelines/paperreprints/. Costs for reprints are below:

Reprint costs		
No of pages	Cost (per 50 copies)	
	First	Each additional
2-4	£225	£125
5-8	£350	£240
9-20	£675	£550
21-40	£1250	£975
>40	£1850	£1550
Cost for including cover of journal issue: £55 per 50 copies		

Queries are marked on your proof like this Q1, Q2, etc. and for your convenience line numbers are indicated like this 5, 10, 15, ...

Query reference	Query	Remarks
Q1	For your information: You can cite this article before you receive notification of the page numbers by using the following format: (authors), Phys. Chem. Chem. Phys., (year), DOI: 10.1039/c1cp22619c.	
Q2	In the sentence beginning 'This morphology leads to...' should 'charge carries' be changed to 'charge carriers'?	
Q3	In the sentence beginning 'Note that TF, TX and XX structures...' the meaning of the phrase 'all of then' is not clear—please clarify.	
Q4	Ref. 20, 31 and 32: Please provide the following details: page number(s).	
Q5	Ref. 39: Can this reference be updated yet? Please supply details to allow readers to access the reference (for references where page numbers are not yet known, please supply the DOI).	

PCCP

Dynamic Article Links

Cite this: DOI: 10.1039/c1cp22619c

www.rsc.org/pccp

PAPER

Easily manufactured TiO_2 hollow fibers for quantum dot sensitized solar cells†

Mahmoud Samadpour,[ab] Sixto Giménez,[a] Azam Iraji Zad,*[bc] Nima Taghavinia[bc] and Iván Mora-Seró*[a]

Received 15th August 2011, Accepted 4th October 2011
DOI: 10.1039/c1cp22619c

TiO_2 hollow fibers with high surface area were manufactured by a simple synthesis method, using natural cellulose fibers as template. The effective light scattering properties of the hollow fibers, originating from their micron size, were observed by diffuse reflectance spectroscopy. In spite of the micrometric length of the TiO_2 hollow fibers, the walls were highly porous and high surface area (78.2 $m^2\ g^{-1}$) was obtained by the BET method. TiO_2 hollow fibers alone and mixed with other TiO_2 pastes were sensitized with CdSe quantum dots (QDs) by Successive Ionic Layer Adsorption and Reaction (SILAR) and integrated as a photoanode in quantum dot sensitized solar cells (QDSCs). High power conversion efficiency was obtained, 3.24% (V_{oc} = 503 mV, J_{sc} = 11.92 mA cm^{-2}, FF = 0.54), and a clear correspondence of the cell performance with the photoanode structure was observed. The unique properties of these fibers: high surface area, effective light scattering, hollow structure to facile electrolyte diffusion and the rather high efficiencies obtained here suggest that hollow fibers can be introduced as promising nanostructures to make highly efficient quantum dot sensitized solar cells.

1. Introduction

Recently inorganic semiconductors have received considerable interest as alternative sensitizers to dye molecules in the so-called quantum dot sensitized solar cells (QDSCs).[1–7] In dye sensitized solar cells, DSCs, molecular dyes are used as light absorbing materials to produce photogenerated electrons, which are injected into a porous matrix of a wide band gap semiconductor (*e.g.* TiO_2). This wide bandgap semiconductor transfers the photogenerated electrons to the external circuit. The dye molecules are regenerated by a redox electrolyte, which acts as hole transporting media.[8]

The quantum dots exhibit unique properties as easy fabrication, tunable absorption spectrum by controlling their size, shape and composition and high molar extinction coefficients.[9,10] Consequently, these materials are extremely interesting for photovoltaic applications. The experimental confirmation of the theoretical predictions of Multiple Exciton Generation (MEG) in colloidal QDs has boosted the interest in semiconductor QD as a light absorbing material in solar cells.[11–13] At this point it is worth mentioning that the MEG effect on colloidal QDs has generated certain controversy regarding its efficiency.[14–16] In spite of the mentioned advantages of QDs, the efficiency of QDSCs is much lower compared to conventional DSCs and the optimal QDSCs configuration has not been obtained yet.[4,7] Improving the poor performance of QDSCs requires the improvement of some issues like: homogeneous assembly of QDs onto the TiO_2 surface, charge injection and recombination, efficient electrolyte and suitable TiO_2 film structure.[1,4,17]

Recently, it was shown that the structure of the TiO_2 films has a crucial role for high efficiency QDSCs; nearly 5% efficiency for CdS/CdSe quantum dot sensitized cells was obtained by controlling the structural properties of TiO_2 photoelectrodes, using a polysulfide liquid electrolyte.[17] To the best of our knowledge this is the highest efficiency reported for QDSCs in the polysulfide liquid electrolyte. A potentially suitable TiO_2 photoanode should satisfy properties as: moderate-high surface area for optimizing the QDs loading, wide and interconnected pores for facile diffusion of the hole transport electrolyte and preventing blockage by QD sensitizers, efficient transport of photoinjected electrons, efficient light harvesting and easy fabrication. At present, different TiO_2 structures have been tested to prepare efficient QDSCs. High surface area TiO_2 nanoparticles have been used in QDSCs for high QDs loading.[17,18] Inverse opals were sensitized with CdSe, encompassing the beneficial effects of ordered interconnected pores in inverse opals together with their light scattering properties.[19,20]

[a] *Grup de Dispositius Fotovoltaics i Optoelectrònics, Departament de Física, Universitat Jaume I, 12071 Castelló, Spain. E-mail: sero@fca.uji.es*
[b] *Institute for Nanoscience and Nanotechnology, Sharif University of Technology, PO Box 11155-8639, Tehran, Iran. E-mail: iraji@sharif.edu*
[c] *Department of Physics, Sharif University of Technology, PO Box 11155-9161, Tehran, Iran*

† Electronic supplementary information (ESI) available. See DOI: 10.1039/c1cp22619c

One dimensional TiO_2 or ZnO nanorods/wires and tubes were used for efficient electron transport in QDSCs.[21–23] In spite of the mentioned advantages of these structures, none of them simultaneously satisfy all the potentially required properties. For example, high surface area nanoparticles lead to high QD loading but also to pore blockage by QDs and intense trapping of electrons can occur at the particle surface and at grain boundaries.[24] Inverse opals exhibit a too low surface area for QD loading, although moderate electron transport could be expected. On the other hand, the synthesis is complicated and the structures are mechanically fragile. One dimensional nanorods/wires and tubes usually suffer from low surface area and manufacturing is not so easy compared to conventional nanocrystalline films for DSCs and QDSCs. In this context, we propose here the use of hollow fibers as interesting nanostructured materials for QDSCs possessing the mentioned advantages altogether. Hollow fibers are synthesized using natural cheap cellulose cotton fibers as template. Simply synthesized hollow fibers have several microns length while their walls are highly porous. The surface area of hollow fibers (78.2 $m^2\ g^{-1}$) is larger compared to conventional nanoparticulate paste (72.9 $m^2\ g^{-1}$) for DSCs and QDSCs. The micrometric size of the fibers shows interesting light scattering properties as characterized by diffuse reflectance spectroscopy. On the other hand, the electronic transport can be potentially improved in these one dimensional hollow fibers. Enhanced electron collection efficiency in hollow fibers compared to mesoscopic films made of spherical nanoparticles has been observed.[25] In addition, effective light scattering and light trapping properties of the hollow fibers for DSCs were also reported recently by some of us.[26] Besides the mentioned properties, "hollow" fibers with wide pores, as confirmed by SEM and BET, prevent pore blockage by QDs and favor the homogeneous electrolyte diffusion into the photoanode. Efficient CdSe QDSCs cells with efficiencies of 3.24% were obtained using hollow fibers. We show that the synthesized hollow fibers can be used as an efficient nanostructure to make highly efficient QDSCs. Scheme 1 illustrates the architecture of some of the different morphologies employed for QDSCs to compare with the hollow fibers.

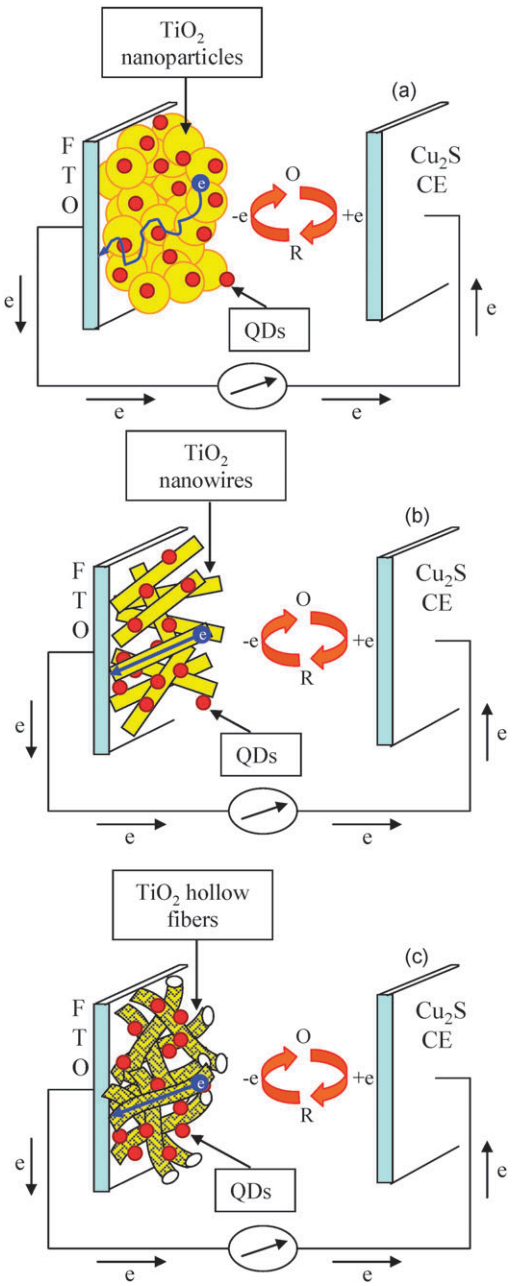

Scheme 1 Schematic view of the effect of the anode structure on the QDSCs performance: (a) photoanode based on TiO_2 nanoparticles, high surface area for sufficient QDs adsorption. The small pores could be blocked during QDs deposition and prevent electrolyte diffusion, non-direct path for electron transport; (b) photoanode based on TiO_2 nanowires, lower surface area compared to nanoparticulated anodes, direct path for electron transport; (c) photoanode based on TiO_2 hollow fibers, the high surface area allows sufficient QDs loading compared to nanoparticulated anodes, direct path for electron transport, hollow structures and porous walls prevent pore blockage during QDs deposition and leads to facile electrolyte diffusion, noticeable light scattering properties.

2. Experimental section

2.1. Synthesis of the hollow fibers

Hollow fibers were synthesized as previously described.[27] Briefly, HCl was added to 1 litre of Milli-Q water until pH was adjusted to 1.8. Then, tetraisopropylorthotitanate (TiPT) was added dropwise to the acidified water while stirring, to make a 0.05 M solution. Adding TiPT leads to a white precipitate which changed to a semi transparent solution after stirring for a few days. The temperature of the solution was adjusted to 60 °C and then about 10 g cotton fiber was dipped into the solution for 5 h. The impregnated fibers were squeezed to remove the extra solution and dried overnight at room temperature. The as-dried fibers were heat treated at 450 °C for 60 min in air. The obtained residue is a white fibrous substance of TiO_2 composition.[26,27]

2.2. Electrode preparation

Three different TiO_2 pastes were used to prepare the electrodes. The first paste is "18NR-T Dyesol" containing 20 nm TiO_2 nanoparticles. This paste is used to make transparent TiO_2

layers, termed below "T". The second paste was based on hollow fibers and is named "F". For this purpose, 1 g of ethyl cellulose was dissolved in 12.5 ml ethanol assisted by ultrasonication. The paste was prepared by milling 0.2 g TiO_2 hollow fibers and 1 ml of prepared ethyl cellulose in ethanol in mortar for 30 minutes while 1 ml of terpineol was added dropwise during the milling process. The third paste is prepared by mixing the 60% wt of paste T with 40% wt of paste F, we name this paste as "X". Nine different electrode configurations were prepared as photoanode in QDSCs by using these three TiO_2 pastes.

The photoanodes were doctor-bladed on transparent conducting fluorine doped tin oxide (FTO) glass substrates (sheet resistance $\approx 10\ \Omega\ \square^{-1}$). The resulting photoelectrodes were sintered at 450 °C, to obtain good mechanical and electrical contact at the interfaces nanoparticle/nanoparticle and nanoparticle/substrate. Before doctor-blading, the FTO substrates were coated by a compact layer of TiO_2 deposited by spray pyrolysis ($\sim$100 nm thick). These electrodes were calcinated at 450 °C for 30 min.

2.3. Electrode sensitization

TiO_2 electrodes were *in situ* sensitized by CdSe QDs grown by SILAR. The SILAR process was carried out following the method developed before.[28] Briefly, 0.03 M $Cd(NO_3)_2$ in ethanol was used as the Cd^{+2} source and the *in situ* prepared 0.03 M Se^{2-} in ethanol was used as Se^{2-} precursor (see ref. 28 for more details). For sensitization, the electrodes were successively dipped into these solutions inside a glove box under a N_2 atmosphere. One SILAR cycle for CdSe consisted of 30-second dipping of the TiO_2 working electrode into the Cd^{2+} precursor and subsequently into the selenide solution, during 30 seconds. After each bath, the photoanode was rinsed by immersion in pure ethanol to remove the chemical residuals from the surface and subsequently dried with a N_2 gun.[18] In order to improve the stability and performance of cells, all the samples were deposited with a ZnS protective coating,[18,29–31] by twice dipping alternatively into 0.1 M $Zn(CH_3COO)_2$ and 0.1 M Na_2S solutions for 1 min/dip, rinsing with Milli-Q ultrapure water between dips.[31]

2.4. QDSC preparation

The cells were prepared by sandwiching a Cu_2S counter electrode and a QD-sensitized photoelectrode using a scotch tape spacer (thickness 50 μm) and permeating with the polysulfide electrolyte. The polysulfide electrolyte was 1 M Na_2S, 1 M S, and 0.1 M NaOH solution in Milli-Q ultrapure water.[32,33] The Cu_2S counter electrodes were prepared by immersing brass in HCl solution at 70 °C for 5 min and subsequently dipping it into polysulfide solution for 10 min, resulting in a porous Cu_2S electrode. The geometric area of the cells was 0.28 cm^2.

2.5. Photoanode and solar cell characterization

Gas adsorption measurements were performed on a Micromeritics ASAP 2020 surface area and porosity analyzer with ASAP 2020 V3.04 E software. Three tests were carried out for each specimen in order to assess the reproducibility of the measurement. The optical absorption spectra of the photoanodes were recorded at 300–800 nm by a Cary 500 UV-VIS Varian spectrometer. *J–V* curves, Impedance Spectroscopy (IS) measurement, Applied Bias Voltage Decay (ABVD)[34] were carried out with a FRA equipped PGSTAT-30 potentiostat from Autolab. *J–V* measurements were carried out using mask (0.24 cm^2) and no antireflective layer was used. Cells were illuminated using a solar simulator at AM1.5 G, where the light intensity was adjusted with an NREL calibrated Si solar cell with a KG-5 filter to one sun intensity (100 mW cm^{-2}). Incident photon to electron conversion efficiency (IPCE) measurements have been performed employing a 150 W Xe lamp coupled with a computer-controlled monochromator, the photocurrent was measured using a nanoamperimeter 70310 from Oriel Instruments. Impedance spectroscopy measurements were carried out under dark conditions applying a 20 mV AC signal with the frequency ranging between 400 kHz and 0.1 Hz at different forward biases.

3. Results and discussion

A representative SEM micrograph of the hollow fibers is shown in Fig. 1(a). The walls of the fibers are highly porous. Consequently, in spite of their micron size, Fig. 1(b), high surface area of the hollow fibers is expected. The surface area of the hollow fibers was measured and compared to that of the TiO_2 nanoparticles which are commonly used in transparent layers for DSSCs and QDSCs. TiO_2 paste with 20 nm nanoparticles (18NR-T, Dyesol) was deposited on the FTO substrate

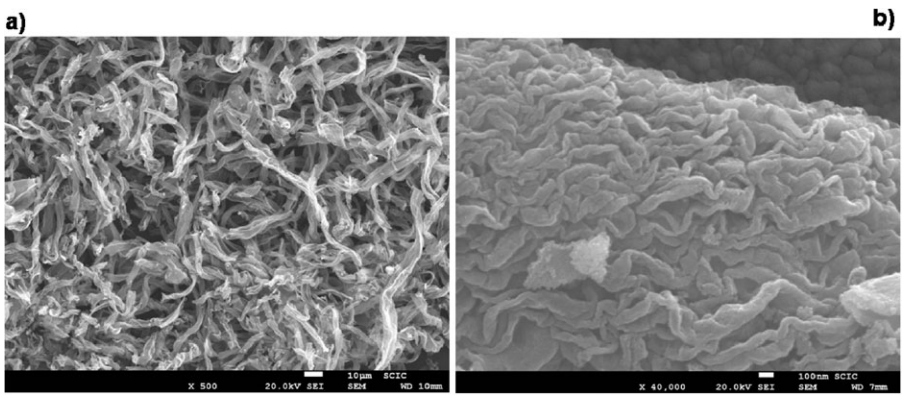

Fig. 1 SEM micrograph from hollow fibers, (a) general view of TiO_2 fibers (scale bar 10 μm), (b) zoom of a fiber porous wall (scale bar 10 nm).

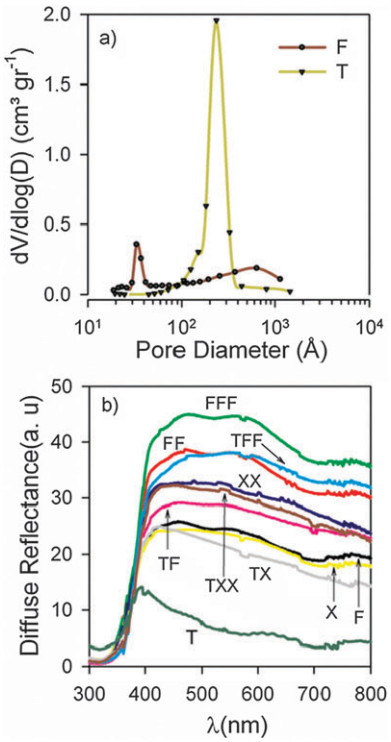

Fig. 2 (a) Pore size distributions derived from BET measurements of T and F structures, (b) diffuse reflectance spectrum of the different TiO_2 structures analyzed containing fibers with T structure.

by Dr Blade and after annealing at 450 °C for 30 min was scratched from the FTO for BET analysis. The surface area of 72.9 m^2 g^{-1} was obtained for this paste, with a pore size distribution around 23 nm, Fig. 2(a). On the other hand, the surface area obtained for the fibers was 78.2 m^2 g^{-1}. The scattering of the BET measurements was below 3% for the hollow fibers and below 1% for the nanoparticles. The pore size distribution peaks around 3.5 nm and a relatively wide distribution of larger pores are observed around 60 nm arising from wall pore structure of the fibers, Fig. 1(b).

Regarding the micron size of the hollow fibers and their high surface area, various structures of TiO_2 photoanodes were designed in order to find the most efficient cells. Three kinds of pastes: T (TiO_2 paste with 20 nm nanoparticles), F (TiO_2 paste with TiO_2 hollow fibers) and X (TiO_2 paste which contained TiO_2 nanoparticles and fibers) were used to prepare the different photoanode structures, see the Experimental section for more details. 1, 2 or 3 layers of TiO_2 paste were doctor bladed on the FTO substrates. We label the structures as "ABC": A, B and C, referring to the type of the paste which is used for the first, second and third layer on the FTO substrate, respectively. For example, the TFF structure means that we have deposited three layers of TiO_2 on FTO: the first layer prepared with T type paste and the second and third layers with F type paste. Fig. S2 in the ESI† shows the cross sectional micrographs of T, F and X films on the FTO substrate.

Nine different structures were tested with hollow fibers or hollow fiber mixtures as TiO_2 photoanode for QDSCs, named: F, FF, FFF, X, XX, TF, TFF, TX, TXX. The thickness of the photoanodes is shown in Table S1 (ESI†). Additionally, the T structure (the only structure without hollow fibers) was manufactured as a reference to compare its light scattering properties with those of the other photoanodes. The light scattering properties of these structures were measured by diffuse reflectance spectroscopy, see Fig. 2(b) where only TiO_2 photoanodes without sensitization were measured. For comparison, Fig. S3 (ESI†) compiles the diffuse reflectance spectra after CdSe sensitization. Considering the structures with one single layer, the F sample exhibits the highest light scattering properties, as can be inferred from the highest diffuse reflectance of this sample at higher wavelengths (where TiO_2 does not absorb). The X sample presents slightly lower scattering compared to F, while the T sample clearly shows the lowest light scattering, see Fig. 2(b). In this sense, a considerable scattering effect could be seen in the structures containing the hollow fibers. As the number of TiO_2 layers increases, the light scattering effect increases accordingly. The light scattering properties of layers made by the fibers are almost four to eight folds, depending on structure, compared to the T structures. The interesting point is that, these hollow fibers do not only exhibit the beneficial scattering effect compared to T structures, but have also higher surface area, compared to the transparent layer, due to the highly porous wall structure, Fig. 1(b).

These nine different structures were sensitized by 7 SILAR cycles of CdSe quantum dots and then coated with ZnS; see the Experimental section. Table 1 shows the solar cell parameters obtained for these QDSCs: photocurrent j_{sc}, open circuit voltage V_{oc}, fill factor FF, and efficiency η, as a function of the different photoanode structures tested under standard conditions (100 mW cm^{-2} AM 1.5G). The results for the transparent paste (TT) and the conventional configuration transparent + scattering pastes (TS)[18] are also included for comparison. In addition to light scattering, increasing the number of TiO_2 layers has two opposing effects. On one hand, light harvesting is increased as the thickness of the photoanode is increased due to higher amount of light absorbing sensitizers. On the other hand, as the thickness of the photoanode is higher, the effective surface of the electrode concomitantly increases, causing an enhancement of recombination. In this sense, a balance among light scattering, QD loading and recombination is mandatory to optimize the QDSC performance as we have

Table 1 Photovoltaic parameters of the QDSCs prepared and analyzed: photocurrent j_{sc}, open circuit voltage V_{oc}, fill factor FF, and efficiency η, as a function of the different cell structures sensitized by SILAR, tested under standard light illumination conditions (100 mW cm^{-2} AM 1.5G). The results for the only transparent paste (TT) and transparent + scattering (TS) are also included for comparison

Cell	V_{oc}/mV	J_{sc}/mA cm^{-2}	FF	E (%)
F	439	3.13	0.48	0.66
FF	509	6.79	0.46	1.59
FFF	486	7.45	0.52	1.88
X	512	10.46	0.51	2.73
XX	503	11.92	0.54	3.24
TT	510	9.92	0.54	2.79
TS[18]	538	13.9	0.51	3.83
TF	514	11.82	0.50	3.04
TFF	433	7	0.48	1.45
TX	511	10.47	0.54	2.89
TXX	468	9.2	0.53	2.28

recently showed.[23] Note, for example that the highest efficiencies have been obtained for XX and TF samples with an intermediate diffuse reflectance, see Fig. 2(b).

The intrinsic properties of each paste are also important for the final solar cell performance. The low efficiency of F, FF and FFF cells, see Table 1, can be mainly ascribed to the low deposition of hollow fibers on the FTO substrate by doctor blade, see Fig. 3(a). In this case there are some fibers randomly deposited on the FTO substrate and there is no good mechanical connection between the individual fibers and between fibers and the FTO substrate. This morphology leads to low quantum dot sensitization and poor transport of charge carries to the external circuit. It is very interesting to compare the F structure with X structures. While the efficiency of the F structure is just 0.66%, Table 1, the efficiency of cells with X structures increased to 2.73% which constitutes a 4-fold enhancement. In this structure, the 20 nm nanoparticles act as a glue crosslinking the fibers and also improving the adhesion with the FTO substrate, Fig. 3(b)–(d). This morphology allows a significantly higher loading of QDS on the photoelectrode, leading to better solar cell performance. Mixing both fibers and nanoparticles (X structures) has the additional beneficial effect of light scattering and facile electron transport provided by the one dimensional hollow fiber structure. The best efficiencies have been obtained with the TX (2.89%), TF (3.04%) and XX (3.24%) structures, although still slightly lower than the conventional configuration transparent + scattering nanoparticles, see Table 1. Taking into account that the fiber paste studied in this work has not been further optimized, the results, in comparison with the commercial pastes TS, are promising.

Representative diffuse reflectance, IPCE and current–voltage (J–V) curves obtained for SILAR sensitized cells are plotted in Fig. 4(a), (b) and (c), respectively. We only show the results for the best configurations (TF, TX, XX) and also for TFF structures since the good efficiency of the TF structure (3.04%) has dramatically decreased to 1.44% after depositing one more layer of hollow fibers on the top of TF structure (TFF structure), see Table 1. The same information for F, FF, FFF, X and TXX can be found in Fig. S3 (ESI†). The measured IPCE for the TF, TX and XX structures sensitized by SILAR is very similar and the IPCE for the TFF structure is clearly decreased compared to these structures, in good agreement with the final obtained photocurrents, Fig. 4(c). Note that TF, TX and XX structures present all of then the same layer thickness.

To better understand the physical characteristics of these solar cells, impedance spectroscopy measurements and ABVD were carried out on QDSCs. Chemical capacitance, C_{μ}, Fig. 5(a), and recombination resistance, R_{rec}, Fig. 5(b), have been obtained from IS measurements using the previously developed model.[18,35,36] C_{μ} is plotted against the voltage drop in the sensitized electrode, V_F. V_F was obtained by subtracting the voltage drop of the series resistance, V_{series} (contacts, counter electrode, electrolyte diffusion), by $V_F = V_{app} - V_{series}$, where V_{app} is the applied potential in the IS measurements. R_{rec} is plotted against the voltage drop in a common equivalent conduction band (CB), V_{ecb}, where the effect of different TiO_2 CB between samples is removed.[36] Plotting R_{rec} against V_{ecb} allows an analysis of the recombination resistance on the basis of an equal density of electrons n (*i.e.* the same distance between the electron Fermi level and the TiO_2 CB). This procedure is

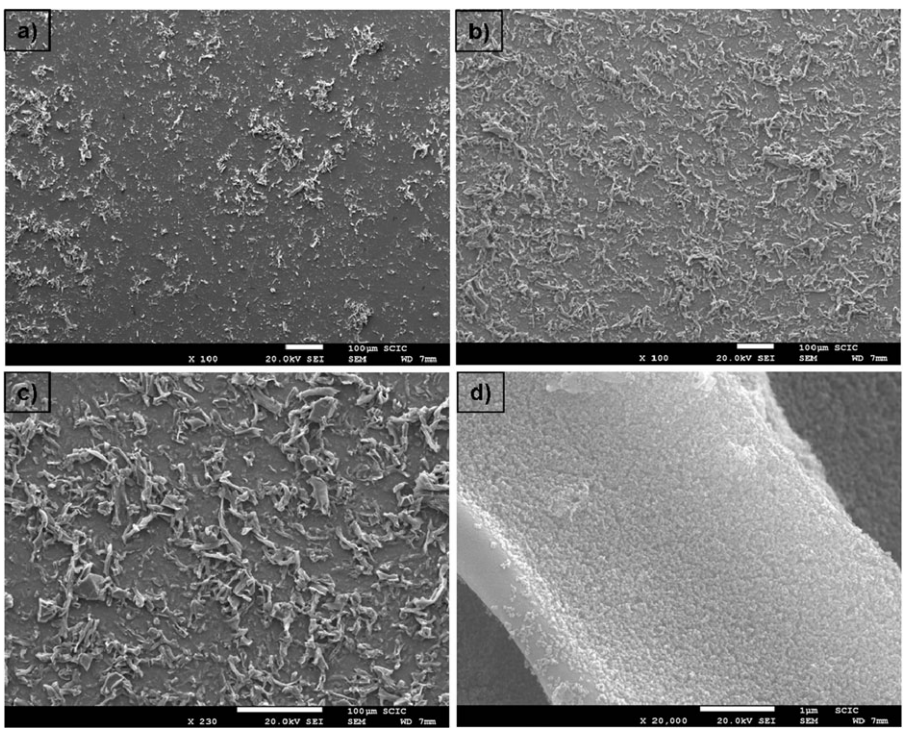

Fig. 3 SEM micrograph of F and X structures, (a) F structure, (b and c) X structure, (d) fibers and nanoparticles mixed in the X structure. Photoinjected electrons into TiO_2 nanoparticles can be transported though one dimensional fibers. Scale bare is 100 micron for a–c and is 1 micron for d.

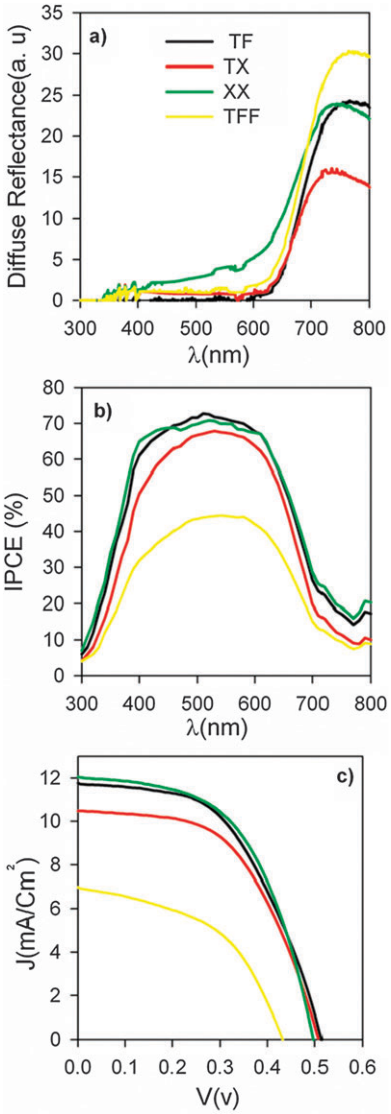

Fig. 4 Diffuse reflectance (a), IPCE (b) and J–V curves (c): for SILAR sensitized cells.

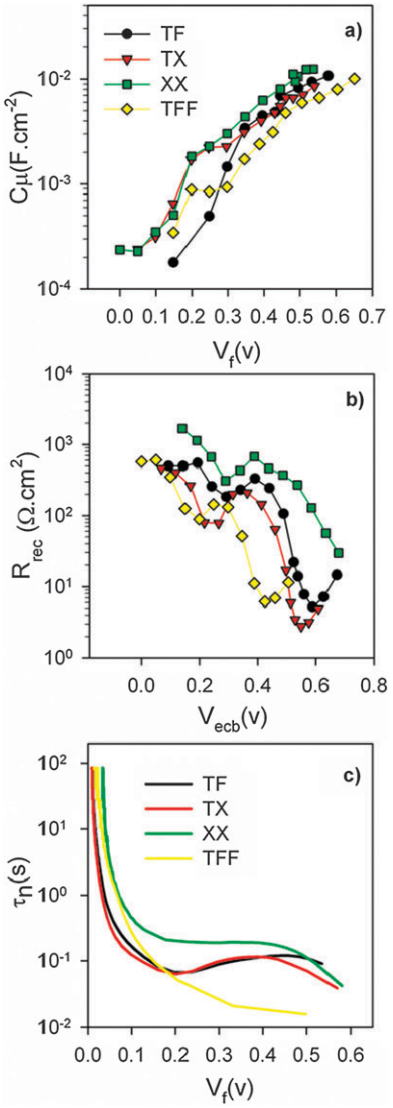

Fig. 5 Chemical capacitance (a), recombination resistance (b) and electron lifetime (c) for QDSCs. Chemical capacitance and recombination resistance have been obtained from IS measurements while electron lifetime[18] from ABVD measurements.[34]

carried out by shifting V_F until the chemical capacitance overlaps; see also Fig. S6 and Table S3 (ESI†). The methods to obtain the dependences against V_F and V_{ecb} from IS measurements have been previously reported.[18,36–38]

Considering the chemical capacitance, Fig. 5(a), all the samples show very similar slopes for C_μ, indicating a similar density of states.[36] On the other hand, C_μ is shifted, indicating a displacement of the TiO_2 CB. Taking the XX sample as a reference, an upward shift of the TiO_2 CB band is observed in the case of TF, TX and especially for TFF samples, Fig. 5(a). After correcting this shift, the TFF samples show the lowest recombination resistance (the highest recombination) observed, see Fig. 5(b). This higher recombination arises from the larger thickness of TFF (15 ± 1 μm) structures (and consequently larger effective surface)[23] compared to the TF, TX and XX samples (11 ± 1 μm), in good agreement with the highest dark current obtained for this cell, see Fig. S5 and Table S1 (ESI†).

In addition, the lower recombination resistance of the TFF cells has been confirmed by comparing the electron lifetime, τ_n, of the samples, Fig. 5(c). τ_n has been obtained from IS and ABVD measurements,[34] under dark conditions. Conversely, the highest efficient cell with XX structure (3.24%), Table 1, has the highest recombination resistance, Fig. 4b, confirmed by τ_n, Fig. 5(c). This fact points out the dramatic role of recombination in the QDSC performance. The valleys observed in R_{rec}, see Fig. 5(b), can be related with recombination through surface states as discussed elsewhere.[5,39]

4. Conclusions

We have synthesized highly porous TiO_2 hollow fibers using natural cellulose fibers as template with a simple method. The unique properties of hollow fibers: high surface area (78.2 $m^2 g^{-1}$), effective light scattering, highly porous structure and hollow structure to facile electrolyte diffusion clearly pushed the efficiency of QDSCs up. We sensitized TiO_2 hollow fibers

and fibers mixed with other TiO_2 pastes, with CdSe QDs grown by SILAR, integrating these electrodes as photoanodes in QDSCs. High power conversion efficiency (η = 3.24%, V_{oc} = 503 mV, J_{sc} = 11.92 mA cm^{-2}, FF = 0.54) was obtained using a mixed paste of fibers and small nanoparticles. The unique properties of these fibers and the rather high efficiencies obtained here suggest that, hollow fibers are promising materials to develop highly efficient QDSCs. It is also highlighted the key role of the photoanode structure in the final cell performance. A rational balance among QD loading, light scattering and recombination is mandatory in order to optimize the performance of the photoanodes for QDSCs.

Acknowledgements

This work was partially supported by the Ministerio de Educación y Ciencia of Spain under the project HOPE CSD2007-00007 (Consolider-Ingenio 2010) JES-NANOSOLAR PLE2009-0042, MAT 2010-19827 and the Ramon y Cajal programme, and by Generalitat Valenciana under project PROMETEO/2009/058.

References

1 G. Hodes, *J. Phys. Chem. C*, 2008, **112**, 17778–17787.
2 P. V. Kamat, *J. Phys. Chem. C*, 2008, **112**, 18737–18753.
3 P. V. Kamat, K. Tvrdy, D. R. Baker and J. G. Radich, *Chem. Rev.*, 2010, **110**, 6664–6688.
4 I. Mora-Seró and J. Bisquert, *J. Phys. Chem. Lett.*, 2010, **1**, 3046–3052.
5 I. Mora-Seró, S. Giménez, F. Fabregat-Santiago, R. Gómez, Q. Shen, T. Toyoda and J. Bisquert, *Acc. Chem. Res.*, 2009, **42**, 1848–1857.
6 B. O'Regan and M. Grätzel, *Nature*, 1991, **353**, 737–740.
7 S. Rühle, M. Shalom and A. Zaban, *ChemPhysChem*, 2010, **11**, 2290–2304.
8 J. Bisquert, D. Cahen, G. Hodes, S. Rühle and A. Zaban, *J. Phys. Chem. B*, 2004, **108**, 8106–8118.
9 A. P. Alivisatos, *Science*, 1996, **271**, 933–937.
10 W. W. Yu, L. Qu, W. Guo and X. Peng, *Chem. Mater.*, 2003, **15**, 2854–2860.
11 R. J. Ellingson, M. C. Beard, J. C. Johnson, P. Yu, O. I. Micic, A. J. Nozik, A. Shabaev and A. L. Efros, *Nano Lett.*, 2005, **5**, 865–871.
12 J. B. Sambur, T. Novet and B. A. Parkinson, *Science*, 2010, **330**, 63–66.
13 R. D. Schaller and V. I. Klimov, *Phys. Rev. Lett.*, 2004, **92**, 186601–186601.
14 M. C. Beard, A. G. Midgett, M. C. Hanna, J. M. Luther, B. K. Hughes and A. J. Nozik, *Nano Lett.*, 2010, **10**, 3019–3027.
15 G. Nair, L.-Y. Chang, S. M. Geyer and M. G. Bawendi, *Nano Lett.*, 2011, **11**, 2145–2151.
16 M. T. Trinh, A. J. Houtepen, J. M. Schins, T. Hanrath, J. Piris, W. Knulst, A. P. L. M. Goossens and L. D. A. Siebbeles, *Nano Lett.*, 2008, **8**, 1713–1718.
17 Q. Zhang, X. Guo, X. Huang, S. Huang, D. Li, Y. Luo, Q. Shen, T. Toyoda and Q. Meng, *Phys. Chem. Chem. Phys.*, 2011, **13**, 4659–4667.
18 V. González-Pedro, X. Xu, I. Mora-Seró and J. Bisquert, *ACS Nano*, 2010, **4**, 5783–5790.
19 L. J. Diguna, M. Murakami, A. Sato, Y. Kumagai, T. Ishihara, N. Kobayashi, Q. Shen and T. Toyoda, *Jpn. J. Appl. Phys., Part 1*, 2006, **45**, 5563–5568.
20 L. J. Diguna, Q. Shen, J. Kobayashi and T. Toyoda, *Appl. Phys. Lett.*, 2007, **91**. Q4
21 S. Huang, Q. Zhang, X. Huang, X. Guo, M. Deng, D. Li, Y. Luo, Q. Shen, T. Toyoda and Q. Meng, *Nanotechnology*, 2010, **21**, 375201.
22 A. Kongkanand, K. Tvrdy, K. Takechi, M. Kuno and P. V. Kamat, *J. Am. Chem. Soc.*, 2008, **130**, 4007–4015.
23 P. Sudhagar, T. Song, D. H. Lee, I. Mora-Seró, J. Bisquert, M. Laudenslager, W. M. Sigmund, W. I. Park, U. Paik and Y. S. Kang, *J. Phys. Chem. Lett.*, 2011, **2**, 1984–1990.
24 N. Guijarro, T. Lana-Villarreal, Q. Shen, T. Toyoda and R. Gómez, *J. Phys. Chem. C*, 2010, **114**, 21928–21937.
25 E. Ghadiri, N. Taghavinia, S. M. Zakeeruddin, M. Grätzel and J. E. Moser, *Nano Lett.*, 2010, **10**, 1632–1638.
26 M. Rahman, F. Tajabadi, L. Shooshtari and N. Taghavinia, *ChemPhysChem*, 2011, **12**, 966–973.
27 M. K. Aminian, N. Taghavinia, A. Iraji-Zad, S. M. Mahdavi, M. Chavoshi and S. Ahmadian, *Nanotechnology*, 2006, **17**, 520–525.
28 H. Lee, M. Wang, P. Chen, D. R. Gamelin, S. M. Zakeeruddin, M. Grätzel and M. K. Nazeeruddin, *Nano Lett.*, 2009, **9**, 4221–4227.
29 N. Guijarro, J. M. Campiña, Q. Shen, T. Toyoda, T. Lana-Villarreal and R. Gómez, *Phys. Chem. Chem. Phys.*, 2011, **13**, 12024–12032.
30 H. J. Lee, J. Bang, J. Park, S. Kim and S. M. Park, *Chem. Mater.*, 2010, **22**, 5636–5643.
31 Q. Shen, J. Kobayashi, L. J. Diguna and T. Toyoda, *J. Appl. Phys.*, 2008, **103**.
32 S. Giménez, I. Mora-Seró, L. Macor, N. Guijarro, T. Lana-Villarreal, R. Gómez, L. J. Diguna, Q. Shen, T. Toyoda and J. Bisquert, *Nanotechnology*, 2009, **20**.
33 G. Hodes, J. Manassen and D. Cahen, *J. Electrochem. Soc.*, 1980, **127**, 544–549.
34 J. Bisquert, A. Zaban, M. Greenshtein and I. Mora-Seró, *J. Am. Chem. Soc.*, 2004, **126**, 13550–13559.
35 F. Fabregat-Santiago, J. Bisquert, G. Garcia-Belmonte, G. Boschloo and A. Hagfeldt, *Sol. Energy Mater. Sol. Cells*, 2005, **87**, 117–131.
36 F. Fabregat-Santiago, G. Garcia-Belmonte, I. Mora-Seró and J. Bisquert, *Phys. Chem. Chem. Phys.*, 2011, **13**, 9083–9118.
37 E. M. Barea, M. Shalom, S. Giménez, I. Hod, I. Mora-Seró, A. Zaban and J. Bisquert, *J. Am. Chem. Soc.*, 2010, **132**, 6834–6839.
38 A. Braga, S. Giménez, I. Concina, A. Vomiero and I. Mora-Seró, *J. Phys. Chem. Lett.*, 2011, **2**, 454–460.
39 I. Hod, V. González-Pedro, Z. Tachan, F. Fabregat-Santiago, I. Mora-Seró, J. Bisquert and A. Zaban, submitted, 2011. Q5